

Hamiltonian light-front field theory within an AdS/QCD basis

J. P. Vary^{a*}, H. Honkanen^a, Jun Li^a, P. Maris^a, S. J. Brodsky^b, A. Harindranath^c,
G. F. de Teramond^d, P. Sternberg^{e †}, E. G. Ng^e, C. Yang^e

^aDepartment of Physics and Astronomy, Iowa State University, Ames, Iowa 50011, USA

^bSLAC National Accelerator Laboratory, Stanford University, Menlo Park, California, USA

^cTheory Group, Saha Institute of Nuclear Physics, 1/AF, Bidhannagar, Kolkata, 700064, India

^dUniversidad de Costa Rica, San José, Costa Rica

^eLawrence Berkeley National Laboratory, Berkeley, California, USA

Non-perturbative Hamiltonian light-front quantum field theory presents opportunities and challenges that bridge particle physics and nuclear physics. Fundamental theories, such as Quantum Chromodynamics (QCD) and Quantum Electrodynamics (QED) offer the promise of great predictive power spanning phenomena on all scales from the microscopic to cosmic scales, but new tools that do not rely exclusively on perturbation theory are required to make connection from one scale to the next. We outline recent theoretical and computational progress to build these bridges and provide illustrative results for nuclear structure and quantum field theory. As our framework we choose light-front gauge and a basis function representation with two-dimensional harmonic oscillator basis for transverse modes that corresponds with eigensolutions of the soft-wall AdS/QCD model obtained from light-front holography.

1. Introduction

Major goals of Hamiltonian light-front field theory include predicting both the masses and transition rates of the hadrons and their structures as seen in high-momentum transfer experiments. So far, the approaches in a discretized momentum basis [1] and in transverse lattice [2, 3, 4] have shown significant promise. The main advantages of Hamiltonian light-front quantum field theory are: (1) one evaluates experimental observables that are non-perturbative and relativistically invariant such as masses, form factors, structure functions, etc.; (2) one evaluates these quantities in Minkowski space; and (3) there is no fermion doubling problem.

Here we present a basis-function approach that exploits recent advances in solving the non-relativistic strongly interacting nuclear many-body problem [5, 6]. Both light-front field theory and nuclear many-body theory face common issues within the Hamiltonian approach - i.e. how to (1) define the Hamiltonian; (2) renormalize to a finite space; (3) solve for non-perturbative observables while preserving as many symmetries as possible; and, (4) take the continuum limit. Nevertheless, Ken Wilson has assessed the advantages of adopting advances in quantum many-body theory and has long advocated adoption of basis function methods as an alternative to the lattice gauge approach [7].

*This work is supported in part by a DOE Grant DE-FG02-87ER40371 and by DOE Contract DE-AC02-76SF00515.

†Currently at ILOG Inc, Incline Village, NV

2. Ab initio Hamiltonian approaches to quantum many-body systems

To solve for the properties of nuclei, self-bound strongly interacting systems, with realistic Hamiltonians, one faces immense analytical and computational challenges. Recently, *ab initio* methods have been developed that preserve all the underlying symmetries and converge to the exact result. The basis function approaches that we adopt here, No Core Shell Model (NCSM)[5] and No Core Full Configuration (NCFC) methods [6], are among the several methods shown to be successful. The former adopts a finite basis-space renormalization method and applies it to realistic nucleon-nucleon (NN) and three-nucleon (NNN) interactions (derived from chiral effective field theory) to solve nuclei with Atomic Numbers $A = 10 - 13$ [8]. Experimental binding energies, spectra, electromagnetic moments and transition rates are well-reproduced. The latter adopts a realistic NN interaction that is sufficiently soft that renormalization is not necessary and binding energies obtained from a sequence of finite matrix solutions may be extrapolated to the infinite matrix limit. Owing to uniform convergence and the variational principle, one is also able to assess the theoretical uncertainties in the extrapolated result. One again obtains good agreement with experiment. The primary advantages of these methods are the flexibility for choosing the Hamiltonian, the method of renormalization/regularization and the basis space. These advantages direct us to adopt the basis function approach in light-front quantum field theory. In a NCSM or NCFC application, one adopts a 3-D harmonic oscillator for all the particles in the nucleus (with harmonic oscillator energy Ω), treats the neutrons and protons independently, and generates a many-fermion basis space that includes the lowest oscillator configurations as well as all those generated by allowing up to N_{max} oscillator quanta of excitations. The single-particle states are formed by coupling the orbital angular momentum to the spin forming the total angular momentum j and total angular momentum projection M_j . The many-fermion basis consists of states where particles occupy the

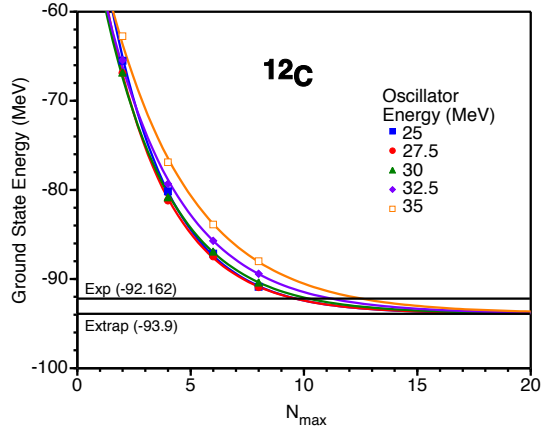


Figure 1. Calculated ground state energy of ^{12}C for $N_{max} = 2-8$ (discrete points) at selected values of the oscillator energy, Ω . For each Ω , the results are fit to an exponential plus a constant, the asymptote, which is constrained to be the same for each curve[6]. We display the experimental ground state energy and the common asymptote. Figure from Ref.[10].

allowed orbits subject to the additional constraint that the total angular momentum projection M_j is a pre-selected value. For the NCSM one also selects a renormalization scheme linked to the many-body basis space truncation while in the NCFC the renormalization is either absent or of a type that retains the infinite matrix problem. Non-perturbative renormalization has been developed to accompany these basis-space methods that preserve all the symmetries of the underlying Hamiltonian including highly precise treatments of the center-of-mass motion. Several schemes have emerged with impressive successes and current research focuses on detailed understanding of the scheme-dependence of convergence rates (different observables converge at different rates) [9]. In the NCFC case, one extrapolates to the continuum limit as illustrated in Fig. 1, where we show results for the ground state of ^{12}C as a function of N_{max} obtained with a realistic NN in-

teraction, JISP16 [11]. The smooth curves portray fits that achieve the desired independence of N_{max} and Ω so as to yield the extrapolated ground state energy. Our assessed uncertainty in the extrapolant is about 2 MeV and there is rather good agreement with experiment within that uncertainty. The largest cases presented in Fig. 1 correspond to $N_{max} = 8$, where the matrix reaches a basis dimension near 600 million. Computation for the $N_{max} = 10$ matrix case is in progress. Large scale calculations like these are performed on leadership-class parallel computers, at Argonne National Laboratory and at Oak Ridge National Laboratory, to solve for the low-lying eigenstates and eigenvectors as well as to carry out evaluation of a suite of experimental observables. For example, one can now obtain the low-lying solutions for $A = 14$ systems with matrices of dimension one to three billion on 8000 to 50000 processors within a few hours of wallclock time. Since the techniques are evolving rapidly [12] and the computers are growing dramatically, much larger matrices are within reach.

3. Basis Light Front Quantized approach

To take full advantage of the similarities with non-relativistic quantum many-body theory in what we will term a ‘‘Basis Light Front Quantized (BLFQ)’’ approach, we adopt a light-front single-particle basis space consisting of the 2-D harmonic oscillator for the transverse modes (radial coordinate ρ and polar angle ϕ) and a discretized momentum space basis for the longitudinal modes. Adoption of this basis is also consistent with recent developments in AdS/CFT correspondence with QCD [13, 14, 15, 16, 17]. We define our light-front coordinates as $x^\pm = x^0 \pm x^3$, $x^\perp = (x^1, x^2)$ and coordinate pair (ρ, ϕ) are the usual cylindrical coordinates in (x^1, x^2) . The variable x^+ is light-front time and x^- is the longitudinal coordinate. We adopt $x^+ = 0$, the ‘‘null plane’’, for our quantization surface.

The 2-D oscillator states are characterized by their principal quantum number n , orbital quantum number m and harmonic oscillator energy Ω . It is also convenient to interpret the 2-D oscillator as a function of the dimensionless radial

length scale variable $\sqrt{M_0\Omega}\rho$ where M_0 has units of mass and ρ is the conventional radial variable in units of length. The properly orthonormalized wavefunctions, $\Phi_{n,m}(\rho, \phi) = \langle \rho\phi | nm \rangle = f_{n,m}(\rho)\chi_m(\phi)$, are given in terms of the Generalized Laguerre Polynomials, $L_n^{|m|}(M_0\Omega\rho^2)$, by

$$\begin{aligned} f_{n,m}(\rho) &= \sqrt{2M_0\Omega} \sqrt{\frac{n!}{(n+|m|)!}} e^{-M_0\Omega\rho^2/2} \\ &\quad \times \left(\sqrt{M_0\Omega}\rho\right)^{|m|} L_n^{|m|}(M_0\Omega\rho^2) \\ \chi_m(\phi) &= \frac{1}{\sqrt{2\pi}} e^{im\phi} \end{aligned} \quad (1)$$

with eigenvalues $E_{n,m} = (2n + |m| + 1)\Omega$. In this 2-D oscillator basis the Fourier transformed wavefunctions have the same analytic structure in both coordinate and momentum space, a feature reminiscent of a plane-wave basis.

The longitudinal modes, ψ_j , in our basis are defined for $-L \leq x^- \leq L$ with both periodic boundary conditions (PBC) and antiperiodic boundary conditions (APBC):

$$\psi_k(x^-) = \frac{1}{\sqrt{2L}} e^{i\frac{\pi}{L}kx^-}, \quad (2)$$

where $k = 1, 2, 3, \dots$ for PBC (neglecting the zero mode) and $k = \frac{1}{2}, \frac{3}{2}, \frac{5}{2}, \dots$ in Eq.(2) for APBC. The full 3-D single particle basis state is defined by the product form

$$\Psi_{k,n,m}(x^-, \rho, \phi) = \psi_k(x^-)\Phi_{n,m}(\rho, \phi). \quad (3)$$

In Figs. 2 and 3 we illustrate some of our basis functions. Fig. 2 presents modes for $n = 1$ of the 2-D harmonic oscillator, and Fig. 3 shows the transverse mode with $n = 1, m = 0$ joined together with the $k = \frac{1}{2}$ longitudinal APBC mode of Eq.(2) and display slices of the real part of this 3-D basis function at selected longitudinal coordinates, x^- . As one increases the orbital quantum number m , pairs of maxima and minima populate the angular dependence of the basis function. Also, as one increases the principal quantum number n , additional radial nodes appear. As explained in [10] and references therein, our choice of basis functions is supported by the the phenomenological success of the ‘‘soft-wall’’ AdS/QCD model [13, 14] which uses a harmonic oscillator potential in the fifth dimension

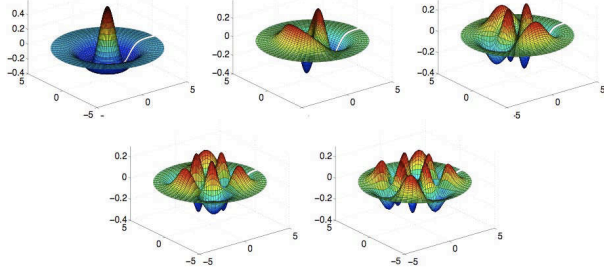


Figure 2. Modes for $n = 1$ of the 2-D harmonic oscillator selected for the transverse basis functions. The orbital quantum number m progresses across the rows by integer steps from 0 in the upper left to 4 in the lower right and counts the pairs of angular lobes. Figure from Ref.[10].

of Anti-de Sitter space to simulate color confinement. The AdS/QCD model, together with light-front holography [15, 16, 17], provides a semiclassical first approximation to strongly coupled QCD. The BLFQ approach in this paper provides a natural extension of the AdS/QCD light-front wavefunctions to multi-quark and multi-gluonic Fock states, thus allowing for particle creation and absorption. By setting up and diagonalizing the light-front QCD Hamiltonian on this basis, we incorporate higher order corrections corresponding to the full QCD theory, and we hope to gain insights into the success of the AdS/QCD model.

4. Cavity mode light-front field theory without interactions

For a first application of the BLFQ approach, we consider a non-interacting QED system confined to a transverse harmonic trap or cavity. The basis functions are matched to the trap so the length scale of the 2-D harmonic oscillator basis is fixed by the trap and finite modes in the longitudinal direction are taken with PBC from Eq.(2) (we omit the zero mode). Since we are ultimately interested in the self-bound states of the system, we anticipate adoption of the NCSM method [5] for factorizing the eigensolutions into simple products of intrinsic and total momentum

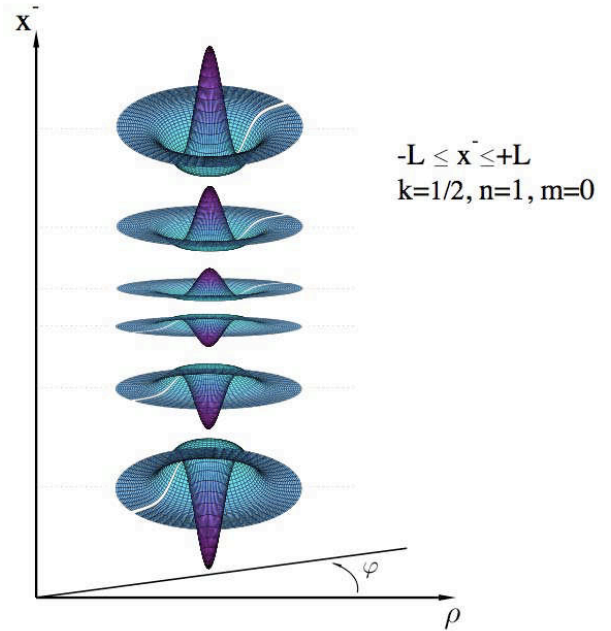


Figure 3. Transverse sections of the real part of a 3-D basis function involving a 2-D harmonic oscillator and a longitudinal mode of Eq.(2) with antiperiodic boundary conditions (APBC). The quantum numbers for this basis function are given in the caption. The basis function is shown for the full range $-L \leq x^- \leq L$. Figure from Ref.[10].

solutions in the transverse direction. That is, with a suitable transverse momentum constraint such as a large positive Lagrange multiplier times the 2-D harmonic oscillator Hamiltonian acting on the total transverse coordinates, the low-lying physical solutions will all have the same expectation value of total transverse momentum squared. Therefore, following Ref.[1] we introduce the total invariant mass-squared M^2 for these low-lying physical states in terms of a Hamiltonian H times a dimensionless integer for the total light front momentum K

$$M^2 + P_\perp P_\perp \rightarrow M^2 + const = P^+ P^- = KH \quad (4)$$

where we absorb the constant into M^2 . The non-interacting Hamiltonian H_0 for this system is de-

finied by the sum of the occupied modes i in each many-parton state with the scale set by the combined constant $\Lambda^2 = 2M_0\Omega$:

$$H_0 = 2M_0P_c^- = \frac{2M_0\Omega}{K} \sum_i \frac{2n_i + |m_i| + 1 + \bar{m}_i^2/(2M_0\Omega)}{x_i}, \quad (5)$$

where \bar{m}_i is the mass of the parton i .

We adopt symmetry constraints and two cutoffs for our many-parton states. For symmetries, we fix the total charge Z , the total azimuthal quantum number M_t , and the total spin projection S along the x^- direction. For cutoffs, we select the total light-front momentum, K , and the maximum total quanta allowed in the transverse mode of each many-parton state, N_{max} . The chosen symmetries and cutoffs are expressed in terms of sums over the quantum numbers of the single-parton degrees of freedom contained in each many-parton state of the system in the following way:

$$\sum_i q_i = Z \quad (6)$$

$$\sum_i m_i = M_t \quad (7)$$

$$\sum_i s_i = S \quad (8)$$

$$\sum_i x_i = 1 = \frac{1}{K} \sum_i k_i \quad (9)$$

$$\sum_i 2n_i + |m_i| + 1 \leq N_{max} \quad (10)$$

where, for example, k_i is the integer that defines the PBC longitudinal modes of Eq.(2) for the i^{th} parton. The range of the number of fermion-antifermion pairs and bosons is limited by the cutoffs in the modes (K and N_{max}). Since each parton carries at least one unit of longitudinal momentum, the basis is limited to K partons. Furthermore, since each parton carries at least one oscillator quanta for transverse motion, the basis is also limited to N_{max} partons. Thus the combined limit on the number of partons is $\min(K, N_{max})$. Only the case with simultaneous increase in both of these cutoffs keeps the problem

physically interesting at higher excitations since this is the only case with unlimited number of partons as both cutoffs go to infinity. In principle, one may elect to further truncate the many-parton basis by limiting the number of fermion-antifermion pairs and/or the number of bosons but we have not elected to do so here.

In a fully interacting application, the actual choice of symmetry constraints will depend on those dictated by the Hamiltonian. For example, with QCD we need to add color and flavor attributes to the single particle states and apply additional symmetries such as requiring all many-parton states to be global color singlets as discussed below. Another example is the choice to conserve total $M_t + S$ rather than conserving each separately as chosen here. It is straightforward, but sometimes computationally challenging, to modify the symmetries in a basis function approach such as we adopt here. However, in order to approach the continuum limit (all cutoffs are removed) as closely as possible with limited computational resources, one works to implement as many of the known symmetries as possible.

In Fig.4 we illustrate how the BLFQ basis-space dimensions rapidly increase as a function of dimensionless state energy for non-interacting QED with massless partons. The states are grouped to form a histogram according to their energy calculated from the chosen Hamiltonian in Eq.(5) where we omit the constant preceding the summation for simplicity. We set $K = N_{max}$, and increase them simultaneously. For simplicity we consider a case with no net charge $Z = 0$, i.e. for zero lepton number. Thus the cavity is populated by many-parton states consisting of fermion-antifermion pairs and photons. The chosen symmetries are $M = 0$ and $S = 0$. As seen from Eqs.(5,9), fixing K but increasing N_{max} leads to a situation where partons carrying large longitudinal momentum fraction become rare, and thus the low-lying modes get eventually maximally populated, leading to saturation. As shown in Ref.[10], the energy at which this saturation occurs, increases with N_{max} . In the case shown here, there is no saturation in state density at low energy. With increasing cutoff, there is a rapid growth in the number of basis states

within each Fock space sector. Overall, there is approximately a factor of 20 increase in the total many-parton basis states with each increase of 2 units in the cutoff. For the non-interacting

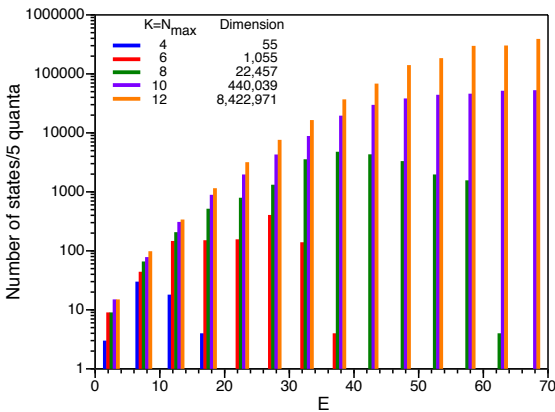


Figure 4. State density as a function of dimensionless state energy E from BLFQ for non-interacting QED in a trap with no net charge and for $K = N_{max}$. The dimensions of the resulting matrices are presented in the legend. The states are binned in groups of 5 units of energy (quanta) where each parton carries energy equal to its 2-D oscillator quanta $(2n_i + |m_i| + 1)$ divided by its light-front momentum fraction ($x_i = k_i/K$). Figure from Ref.[10].

Hamiltonian the scale is available through an overall factor $\Lambda^2 = 2M_0\Omega$ as described above. Without interactions and the associated renormalization program, one cannot relate the scales at one set of (K, N_{max}) values to another. Ultimately, one expects saturation will arise with interaction/renormalization physics included as one increases the set of (K, N_{max}) values.

These state densities could serve as input to model the statistical mechanics of the system treated in the microcanonical ensemble. Of course, interactions must be added to make the

model realistic at low temperatures where correlations are important. After turning on the interactions, the challenge will be to evaluate observables and demonstrate convergence with respect to the cutoffs (N_{max} and K). Independence of the basis scale, Ω , must also be obtained as N_{max} increases Ref.[18]. These are the standard challenges of taking the continuum limit.

The approach can be extended to QCD by implementing the SU(3) color degree of freedom for each parton - 3 colors for each fermion and 8 for each boson. For simplicity, we restrict the present discussion to the situation where identical fermions occupy distinct space-spin single-particle modes. We consider two versions of implementing the global color-singlet constraint for the restricted situation under discussion here. In both cases we enumerate the color space states to integrate with each space-spin state of the corresponding partonic character. In the first case, we follow Ref. [19] by enumerating parton states with all possible values of SU(3) color. Thus each space-spin fermion state goes over to three space-spin-color states. Similarly, each space-spin boson state generates a multiplicity of eight states when SU(3) color is included. We then construct all many-parton states having zero color projection. Within this basis one will have both global color singlet and color non-singlet states. The global color-singlet states are then isolated by adding a Lagrange multiplier term in many-parton color space to the Hamiltonian so that the unphysical color non-singlet states are pushed higher in the spectrum away from the physical color single states. To evaluate the increase in basis space dimension arising from this treatment of color, we enumerate the resulting color-singlet projected color space states and display the results as the upper curves in Fig. 5.

In the second case, we restrict the basis space to global color singlets and this results in the lower curves in Fig. 5. The second method produces a typical factor of 30-40 lower multiplicity at the upper ends of these curves at the cost of increased computation time for matrix elements of the interacting Hamiltonian. That is, each interacting matrix element in the global color-singlet basis is a transformation of a submatrix in the zero color

projection basis. Either implementation dramatically increases the state density over the case of QED, but the use of a global color-singlet constraint is clearly more effective in minimizing the explosion in basis space states.

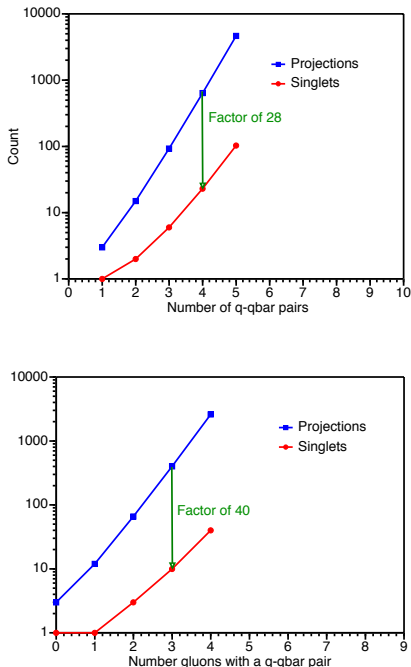


Figure 5. Number of color space states that apply to each space-spin configuration of selected multi-parton states for two methods of enumerating the color basis states. The upper curves are counts of all color configurations with zero color projection. The lower curves are counts of global color singlets. Figures from Ref.[10].

5. Elements of the interacting theory

In the interacting theory a primary concern will be to manage the divergent structure of the theory. There are two possible locations for divergences in a Hamiltonian basis function approach:

(1) the matrix elements themselves diverge, or
 (2) the eigenvalues diverge as one or more cut-offs are removed. In our planned cavity field theory application with interactions, we will manage these divergences with the help of suitable counterterms and boundary conditions. The infrared divergences in light-front momentum arising in both the fermion to fermion-boson vertex as well as in the instantaneous fermion-boson interaction are expected to be well-managed by previously defined counterterms [3] suitably transcribed for the transverse basis functions we have adopted. We anticipate this prescription will work since the longitudinal modes we adopt are similar to those used in Ref. [3]. Finally, we expect the transverse ultraviolet divergences to be suitably-managed with our basis function selection. As an alternative scheme for comparison we also plan to adopt a second approach that involves a recently proposed sector-dependent coupling constant renormalization scheme [20]. Another alternative which we may adopt uses the Pauli-Villars regulator [21].

Since we are introducing a basis-function approach for the transverse degrees of freedom, we need to investigate convergence rates with increased cutoff of the transverse modes N_{max} . Here, in a simple set of examples, we outline how we can search for additional sources of divergence with the help of a perturbation theory analysis. For a first investigation, we have examined the behavior of various sets of matrix elements for the fermion to fermion-boson vertex. For the purpose of this investigation, we adopt periodic (antiperiodic) boundary conditions for the longitudinal modes of the bosons (fermions) and we hold spin projections fixed for initial and final states. We then adopt specific values for the longitudinal momentum fractions observing the conservation rule. The trends we examine should not be sensitive to the specific values adopted.

Consider the second order energy shift, ΔE , induced on a single parton in the transverse mode (n, m) by its coupling V to partons in higher energy transverse modes (n', m') :

$$\Delta E_{n,m} \approx \int \frac{|\langle n, m | V | n', m' \rangle|^2}{E_{n,m} - E_{n',m'}} \rho(\bar{n}') d\bar{n}', \quad (11)$$

where

$$\bar{n}' = 2n' + |m'| \quad (12)$$

$$E_{n',m'} = (\bar{n}' + 1)\Omega \quad (13)$$

$$\rho(\bar{n}') = \bar{n}' + 1 \quad (14)$$

and the degeneracy is taken into account in ρ .

Thus, according to perturbation theory, we expect a UV divergence if the matrix element falls off too slowly with increasing \bar{n}' . In particular, if the matrix element falls approximately as $(\bar{n}')^{-\frac{1}{2}}$, then we expect a logarithmic divergence since the integrand will have a net $(\bar{n}')^{-1}$ dependence. If the falloff is even slower then we encounter a more serious divergence. Another possible source of a log divergence could arise within the selected sum over m' in which case ρ , the level density factor in the integrand, is unity. Then, if the matrix elements for fixed n, n' are approximately constant with increasing m' , we again find a log divergence in the sum over m' .

We portray in Figs.6 and 7 representative sequences of how these off-diagonal matrix elements behave as one increases the difference in the initial and final state principal quantum numbers. We also portray two interesting cases where the fermion and fermion-boson principal quantum numbers track each other, cases that do not enter a perturbative analysis. Note that we have limited the illustrations to the transverse components of our matrix elements. We also select cases where the fermion spin is flipped, cases that are proportional to the fermion mass. We set the fermion mass to unity so the results are expressed in units of the fermion mass. We further limit our presentation to the case where all partons remain in the orbital projection quantum number zero state and the 2-parton (fermion-boson) states have each parton in the same transverse state. For the non-perturbative illustrative cases, we display the matrix element trends where all partons remain in the same transverse mode, $(n, 0)$.

When the single fermion state has an even value of the principal quantum number n as shown in Fig. 6, the matrix elements appear to be well-behaved either when the 2-parton configuration is the lowest accessible case ($(0000|)$) or when the each of the two partons resides in the state with

the same principal quantum number as the single fermion state. We demonstrate anticipated good convergence with increasing n by showing that the matrix elements, when multiplied by $\sqrt{n+1}$, still fall with increasing n . For the case when the single fermion state has an odd value of the principal quantum number n as shown in Fig. 7, the situation is somewhat different. For the matrix element set entering a perturbative analysis, the matrix elements fall to zero with increasing n sufficiently fast that multiplying by $\sqrt{n+1}$ does not significantly distort the trend to zero. However, the large n behavior of the fermion-boson matrix element, with all partons at the same n , is seen to go approximately as $\sqrt{n+1}$. This is best seen in Fig. 7 where the matrix elements are multiplied by $\sqrt{n+1}$ and the result appears to be a nonzero constant at large n . Since this trend does not appear in a second order perturbation theory analysis, we must await the full Hamiltonian diagonalization to better understand its role in the convergence with increasing N_{max} . To date, we have found no matrix element trends with increasing transverse energy that would imply new divergences. All such matrix elements sets we examined, within a perturbative analysis, fall faster than $1/\sqrt{n'}$. Also, we found no sets that remained constant with increasing m' (and thus m) holding n, n' fixed. As a result of this initial analysis, we anticipate that straightforward adoption of counterterm methods previously introduced [3] will be sufficient for managing the identified divergences in BLFQ.

As another example of the interacting cavity mode QED, we present in Fig.8 the eigenvalue spectra for a Hamiltonian matrix that includes lepton and lepton-photon Fock spaces. The leptons are now massive with $\bar{m}_l = 0.511$ MeV, and the HO parameters are $\Omega = 0.1$ MeV and $M_0 = \bar{m}_l$. The other basis parameters are chosen as $K = 3$, $N_{max} = 2$ and $M_j = 1/2$. The eigenvalues are shown as a function of the strength of the coupling with respect to the coupling at QED, with $g_{\text{QED}} = \sqrt{4\pi\alpha}$. Since the instantaneous fermion interaction term only contributes when all the leptons and photons of the process have their spins aligned, this particular case only involves the photon emission vertex interaction

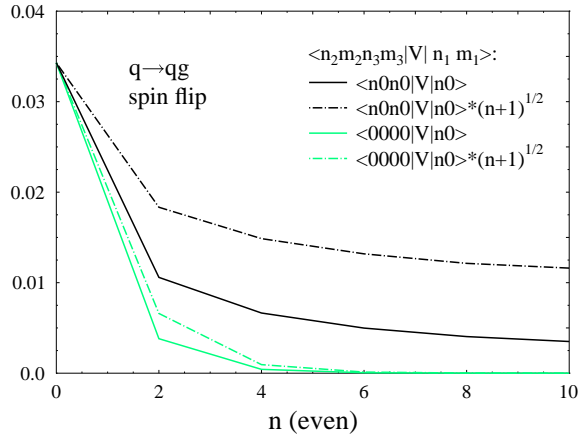


Figure 6. Behavior of representative fermion to fermion-boson matrix elements in BLFQ. The quantum numbers specifying the parton transverse modes (n_i, m_i) in the matrix elements are given in the legend. Only the transverse mode contributions to the matrix elements are shown. Results are also shown with a multiplicative factor of $\sqrt{n+1}$ applied to help search for a logarithmic divergence by obtaining a resulting flat behavior, when it occurs. Overall matrix element normalization depends on the specific values of light-front momentum fractions carried by the interacting partons. Figure from Ref.[10].

(see e.g. Ref.[22]). Application of the sector-dependent renormalization [20] will shift these eigenvalues such that the lowest one will obtain the value $E_0 = \frac{\bar{m}^2 + M_0 \Omega}{K}$, where \bar{m} is the mass of the lowest state fermion. As we increase the cutoffs K, N_{max} , the evaluation of the electron anomalous magnetic moment will serve as an important precision test for our method [22].

6. Conclusions

Following successful methods of *ab initio* nuclear many-body theory, we have introduced a basis light-front quantization (BLFQ) approach to Hamiltonian quantum field theory. With a cavity mode treatment of massless non-interacting QED

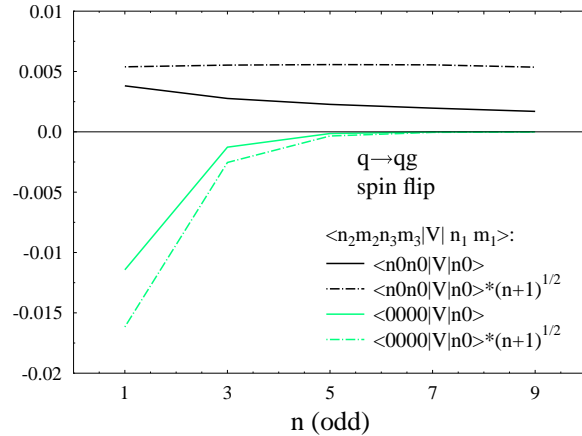


Figure 7. As in Fig.6. Note that for one of the cases shown here, the resulting matrix elements vanish with increasing n while the other case shows a constant trend but does not enter a second-order perturbative analysis. Figure from Ref.[10].

we showed how the number of many-parton basis states exhibit a dramatic rise as the cutoffs are elevated. In order to extend our method to QCD, we presented two methods for treating the color degree of freedom and demonstrated sample measures of the efficiency gains for global color singlets over basis states with color-singlet projection alone. For the interacting cavity mode QED we outlined our approach to managing the expected divergences in a manner that will preserve all the symmetries of the theory. An initial inspection of the interaction vertices of QED in the BLFQ approach shows smooth behaviors that, following a second-order perturbative analysis, are not expected to lead to divergences. It appears that the cavity mode treatment, with the type of basis spaces we have selected, will encounter the divergences in a more subtle fashion as cutoffs are elevated. The evaluation of the electron anomalous magnetic moment will be an important test to our method as we expand our basis space.

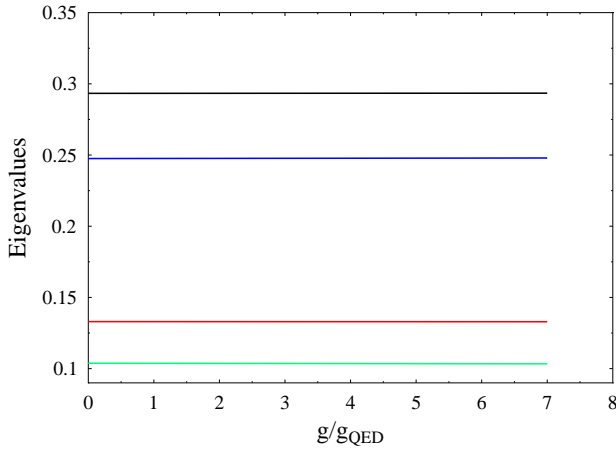


Figure 8. Eigenvalues of a cavity mode QED Hamiltonian, which includes lepton and lepton-photon Fock spaces, as a function of the strength of the coupling ($g_{\text{QED}} = \sqrt{4\pi\alpha}$). The HO parameters are $\Omega = 0.1$ MeV and $M_0 = 0.511$ MeV, and the other basis parameters are $K = 3$, $N_{\text{max}} = 2$ and $M_j = 1/2$.

REFERENCES

1. H. C. Pauli and S. J. Brodsky, *Phys. Rev. D* **32**, (1985)1993; S. J. Brodsky, H. C. Pauli and S. S. Pinsky, *Quantum Chromodynamics and Other Field Theories on the Light Cone*, *Phys. Reports* **301** (1998) 299 [[hep-ph/9705477](#)].
2. M. Burkardt and S. Dalley, *Prog. Part. Nucl. Phys.* **48**, 317 (2002) [[hep-ph/0112007](#)].
3. D. Chakrabarti, A. Harindranath and J. P. Vary, *Phys. Rev. D* **69**, (2004) 034502 [[hep-ph/0309317](#)].
4. D. Grunewald, E. M. Ilgenfritz, E. V. Prokhvatilov and H. J. Pirner, *Phys. Rev. D* **77** (2008) 014512.
5. P. Navrátil, J. P. Vary and B. R. Barrett, *Phys. Rev. Lett.* **84** (2000) 5728; *Phys. Rev. C* **62** (2000) 054311.
6. P. Maris, J. P. Vary and A. M. Shirokov, *Phys. Rev. C* **79** (2009) 014308, [[nucl-th/0808.3420](#)]
7. K. G. Wilson, *Nucl. Phys. Proc. Suppl.* **17**, 82 (1990).
8. P. Navrátil, V. G. Gueorguiev, J. P. Vary, W. E. Ormand and A. Nogga, *Phys. Rev. Lett.* **99** (2007)042501 [[nucl-th/0701038](#)].
9. S. K. Bogner, R. J. Furnstahl, P. Maris, R. J. Perry, A. Schwenk and J. P. Vary, *Nucl. Phys. A* **801**, (2008) 21 [[nucl-th/0708.3754](#)].
10. J. P. Vary *et al.*, arXiv:0905.1411 [nucl-th].
11. A. M. Shirokov, J. P. Vary, A. I. Mazur and T. A. Weber, *Phys. Letts. B* **644** (2007) 33 [[nucl-th/0512105](#)].
12. P. Sternberg, E. G. Ng, C. Yang, P. Maris, J. P. Vary, M. Sosonkina and H. V. Le, in Proceedings of the 2008 ACM/IEEE Conference on Supercomputing (Austin, Texas, November 15 - 21, 2008). Conference on High Performance Networking and Computing. IEEE Press, Piscataway, NJ, 1-12. DOI=<http://doi.acm.org/10.1145/1413370.1413386>.
13. A. Karch, E. Katz, D. T. Son and M. A. Stephanov, *Phys. Rev. D* **74**, 015005 (2006) [[arXiv:hep-ph/0602229](#)].
14. J. Erlich, E. Katz, D. T. Son and M. A. Stephanov, *Phys. Rev. Lett.* **95**, 261602 (2005) [[arXiv:hep-ph/0501128](#)].
15. G. F. de Teramond and S. J. Brodsky, *Phys. Rev. Lett.* **102**, 081601 (2009) [[arXiv:0809.4899 \[hep-ph\]](#)].
16. S. J. Brodsky and G. F. de Teramond, *Phys. Lett. B* **582**, 211 (2004) [[arXiv:hep-th/0310227](#)].
17. J. Polchinski and M. J. Strassler, *Phys. Rev. Lett.* **88**, 031601 (2002) [[arXiv:hep-th/0109174](#)].
18. S. Coon, *et al.*, work in progress.
19. R. J. Lloyd and J. P. Vary, *Phys. Rev. D* **70** (2004) 014009 [[hep-ph/0311179](#)].
20. V. A. Karmanov, J.-F. Mathiot and A. V. Smirnov, *Phys. Rev. D* **77** (2008) 085028 [[hep-th/0801.4507](#)]
21. S. J. Brodsky, J. R. Hiller and G. McCartor, *Phys. Rev. D* **58**, 025005 (1998) [[arXiv:hep-th/9802120](#)].
22. H. Honkanen *et al.*, to be published.